PCCP

ROYAL SOCIETY OF CHEMISTRY

PAPER

View Article Online
View Journal | View Issue

Cite this: *Phys. Chem. Chem. Phys.*, 2021, **23**, 10303

Understanding the magnetization blocking mechanism in N_2^{3-}-radical-bridged dilanthanide single-molecule magnets†

Giang T. Nguyen * and Liviu Ungur *

Received 31st January 2021,
Accepted 8th April 2021

DOI: 10.1039/d1cp00452b

rsc.li/pccp

Herein, we report a theoretical investigation of the electronic structure and magnetic properties in $[(Cp_2^{Me4H}Ln(THF))_2(\mu\text{-}N_2^{\bullet})]^-$ and $[(Cp_2^{Me4H}Ln)_2(\mu\text{-}N_2^{\bullet})]^-$ (THF = tetrahydrofuran, Cp^{Me4H} = tetramethylcyclopentadienyl, Ln = Tb, Dy) complexes [as reported in Demir *et al.*, *Nat. Commun.*, **8**, 1–9, 2144 (2017)]. By *ab initio* methods, their magnetic blocking behaviors are successfully characterized allowing elucidation of the origin of the two blocking barriers observed experimentally. In addition, a detailed analysis of exchange wave functions explains why the blocking barrier of the Tb complexes is roughly twice as large as that of the Dy analogues, a fact which appears to be a general trend exhibited in this family of compounds.

1 Introduction

Single-molecule magnets (SMMs) are molecules that exhibit magnetic hysteresis below a critical temperature. The first molecule displaying such behavior is Mn_{12} which possesses a blocking energy barrier of $U_{eff} = 51\ cm^{-1}$ and magnetic hysteresis up to 2.5 K.[1,2] Because of these intriguing properties, they are potentially applicable in high-density information storage,[2,3] molecular toroics,[4] molecular spintronics[5,6] and quantum computation.[7–9] The vital prerequisite for an arbitrary compound to display SMM behavior is that its ground state displays magnetic bistability, which is a result of magnetic anisotropy. Thus, strongly anisotropic ions, such as transition-metal (3d) and lanthanide (4f) (and to a lesser extent actinide ions (5f)) are utilized in the field. Systems containing 3d-ions are usually at the strong exchange limit such that the energy separation between some low-lying levels by the exchange interaction is much larger than that of the crystal-field (CF) effect. In this case, the blocking energy barrier can be approximated as $U_{eff} = |D|S^2$.[10] On the other hand, lanthanide complexes also have attracted great attention owing to their large single-ion anisotropy arising from the combination of spin–orbit coupling and the CF effect. Over the past decade, the performance of 4f-SMMs has been improved drastically.[11–23] Currently, the $[(Cp^{iPr5})Dy(Cp^*)]^+$ single-ion magnet (SIM) reported in 2018 exhibits the highest blocking energy barrier of 2217 K and magnetic hysteresis at a record temperature of 80 K.[24]

Besides enhancing the magnetic axiality of individual magnetic sites,[25–27] coupling multiple magnetic ions represents an alternative route towards the development of the field. By this approach, the total magnetic moment could be increased, and thus improve the magnetization blocking behavior. It has been shown that a strong exchange interaction is able to suppress various mechanisms of magnetic relaxation, such as quantum tunneling of magnetization (QTM).[28,29] However, since the 4f orbitals of lanthanide ions are shielded by the outermost electronic shells (5p and 5s), the common intra-molecular magnetic exchange interaction is relatively weak. To promote the interaction, bridging the lanthanide centers by a radical ligand has proved to be a fruitful strategy. Due to the fact that the radical's HOMO orbital is relatively diffuse, it is able to penetrate the electron density of the outer shells of the metal ions, enhancing the coupling with the 4f magnetic shells *via* the superexchange mechanism.[30,31] Indeed, a series of N_2^{3-}-radical-bridged dilanthanide complexes reported by Rinehart *et al.* have displayed an exceptionally strong exchange interaction of a few orders of magnitude larger than the usual complexes.[32] As a result, a terbium compound has shown a 100 s. blocking temperature of 13.9 K.[33] Furthermore, it was also the first molecule whose exchange interaction was studied by inelastic neutron scattering technique.[34] Over the past few years, research on radical-lanthanide systems has been conducted intensively. Many complexes of this type have been synthesized that show SMM behavior. For instance, $[\{(\eta^5\text{-}Cp^*)_2Dy\}_2(\mu\text{-ind})]^{n-}$ (n = 0, 1) possess blocking barriers of 39 cm^{-1} and 35 cm^{-1}, respectively;[35] $[(Cp_2^*Ln)_2(\mu\text{-bpym}^{\bullet})]^*$ (Ln = Tb, Dy)

Department of Chemistry, Faculty of Science, National University of Singapore, Block S8 Level 3, 3 Science Drive 3, 117543, Singapore.
E-mail: nguyengiang@u.nus.edu, chmlu@nus.edu.sg; Tel: +65 83691865

† Electronic supplementary information (ESI) available. See DOI: 10.1039/d1cp00452b

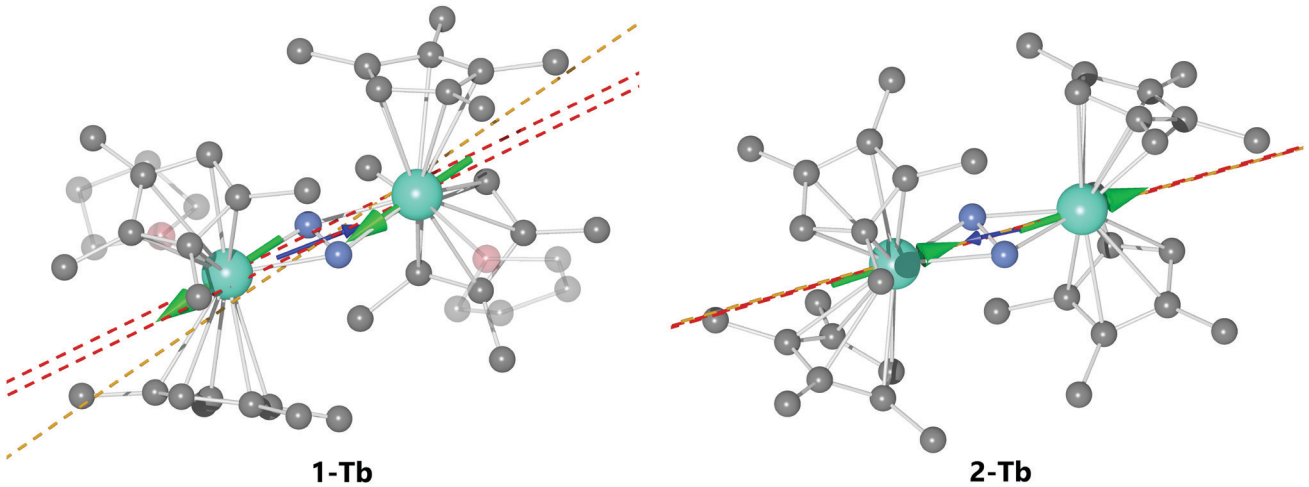

Fig. 1 Molecular structure of **1-Tb** (left) and **2-Tb** (right). Cyan, blue, red and gray spheres illustrate Tb, N, O and C atoms, respectively. Hydrogen atoms are omitted and THF groups are faded for clarity. Red dashed lines indicate the magnetic anisotropy axis of the ground doublet on each Ln ion while the yellow dashed line indicates the ground exchange doublet. Green and blue arrows demonstrate the magnetic moments of the Ln ions and the radical, respectively.

show U_{eff} = 44 and 87.8 cm^{-1}.[36] Besides nitrogen-based radicals,[32,33,35–40] the tetraoxolene ligand can be utilized to enhance the coupling as well.[41–43] So far, the top-performing SMM in this family is $[\mathrm{K(crypt\text{-}222)}][(\mathrm{Cp_2}^{\mathrm{Me4H}}\mathrm{Tb})_2(\mu\text{-}\mathrm{N_2}^{\bullet})]$ which retains magnetization for 100 s. at the temperature of 20 K.[40]

Despite of the fact that the synthesis of radical-lanthanide complexes has been progressively developed,[30,44,45] their microscopic picture remains ambiguous owing to the intricate interplay between the local CF effect and the exchange interaction. Herein, we report a computational investigation for the two recently synthesized series $[(\mathrm{Cp_2}^{\mathrm{Me4H}}\mathrm{Ln(THF)})_2(\mu\text{-}\mathrm{N_2}^{\bullet})]^{-}$ (THF = tetrahydrofuran, $\mathrm{Cp}^{\mathrm{Me4H}}$ = tetramethylcyclopentadienyl, Ln = Tb (**1-Tb**), Dy (**1-Dy**)) and $[(\mathrm{Cp_2}^{\mathrm{Me4H}}\mathrm{Ln})_2(\mu\text{-}\mathrm{N_2}^{\bullet})]^{-}$ (Ln = Tb (**2-Tb**), Dy (**2-Dy**)) (Fig. 1 and Fig. S1–S3, ESI†).[40] Based on the obtained data, the magnetic blocking mechanism is elucidated to shed some light on the microscopic nature of such complexes.

2 Theoretical approach

The ground *J*-multiplet of the $\mathrm{Ln^{3+}}$–$\mathrm{N_2}^{3-}$–$\mathrm{Ln^{3+}}$ system can be described by the following Hamiltonian:[31]

$$\hat{H} = \hat{H}_{\mathrm{CF}} + \hat{H}_{\mathrm{CF}}{}' + \hat{H}_{\mathrm{ex}}, \tag{1}$$

$$\hat{H}_{\mathrm{CF}} = \sum_{kq} \alpha_n B_k^q O_k^q(J), \tag{2}$$

$$\hat{H}_{\mathrm{CF}}' = \sum_{i=1,2} \sum_{kq} \mathcal{J}_{kq00} \frac{O_k^q(\hat{J}_i)\hat{I}}{O_k^0(J)}, \tag{3}$$

$$\hat{H}_{\mathrm{ex}} = \sum_{i=1,2} \sum_{kqq'} \mathcal{J}_{kq1q'} \frac{O_k^q(\hat{J}_i)\hat{S}_{q'}}{O_k^0(J)S}, \tag{4}$$

where H_{CF} expresses the local CF of the lanthanide ions given by the surrounding ligands;[46] $H_{\mathrm{CF}}{}'$ is the covalent CF arising from the electron delocalization between $\mathrm{Ln^{3+}}$ and $\mathrm{N_2}^{3-}$; H_{ex} characterizes the exchange interaction between them. The Steven matrix elements are calculated as:[47]

$$O_k^q = \sum_{MM'} \frac{C_{JM'kq}^{JM}}{C_{JJk0}^{JJ}} |JM\rangle\langle JM'|, \tag{5}$$

where $C_{j_2 m_2 kq}^{j_1 m_1}$ are the Clebsch–Gordan coefficients.[48] While eqn (2) is treated adequately by *ab initio* methods, eqn (3) and (4) emerged from the exchange interaction are computed semi-empirically.

It is noteworthy that because of the giant exchange interaction, instead of mixing only the ground CF doublet on each Ln center, the mixture involves the whole ground CF multiplet.[49–52] As a result, the non-negligible exchange parameters are up to rank $k = 7$ and projection $|q| = 5$. The exchange interaction is governed by the superexchange mechanism,[53,54] which has been investigated theoretically by a combination of computational methods and the microscopic Hubbard models elsewhere.[31] The result shows that the superexchange originates from the overlap between the $4f_{xyz}$ orbital(s) of the lanthanide ion and the π^* next LUMO orbital of the $\mathrm{N_2}^{3-}$ radical. It is estimated that the dominant contribution to this process is kinetic exchange; the other terms such as Goodenough's mechanism,[55] direct exchange and magnetic dipolar interaction are expected to have a significantly smaller effect than the kinetic exchange. The investigation also concludes that exchange coupling is not always favourable to magnetization blockage. In some circumstances, it reduces the magnetic axiality of the low-lying exchange states and limits the blocking barrier to the first-excited level.[31]

3 Computational details

In this study, according to the crystallographic information files (CIFs), the Ln–N bond lengths vary from 2.23 Å to 2.27 Å[40]

while those of the complexes studied previously[31] are around 2.22–2.25 Å.[32,33] Therefore, it is assumed that the surrounding ligands does not affect much the magnetic core, and its exchange nature remains the same. The assumption will be validated later by the comparison of the computed exchange parameters. Thus, the exchange model in ref. 31 is utilized such that the transfer parameter (t) and the energy difference between the 4f and π^* orbitals (Δ) remains unchanged while the only unknown parameter, the minimal electron promotion energy (U_0), is varied to reproduce the experimental magnetic susceptibility.

Molecular structures of the complexes were taken from the corresponding X-ray diffraction data.[40] Calculations of electronic states were performed within the MOLCAS 8.4 program.[56,57] Due to the current computational limitation, one of the paramagnetic centers was substituted by the analogous diamagnetic center Lu^{3+}. To simulate the electrostatic effect arising from the unpaired electron in the N_2^{3-} radical, a point charge $-0.5e$ (e = 1.602 × 10^{-19} C) was placed on each N atom. CASSCF calculations[58] were carried out with an active space including all electrons in seven 4f orbitals. The ANO-RCC basis sets[59] were utilized with the VTZP contracted sets for the atoms surrounding the paramagnetic center and the VDZ contracted sets for the others. To include a spin–orbit interaction in the ground J-multiplet, the Restricted Active Space State Interaction (SO-RASSI)[60] was employed mixing 7 septet, 140 quintet, 113 triplet, and 123 singlet states for Tb^{3+}, and 21 sextet, 128 quartet, and 130 doublet states for Dy^{3+}.

The SINGLE_ANISO module[61] computed magnetic properties of the mononuclear fragments. The spin–orbit wave functions obtained from the preceding calculations were constructed into the pseudospin Hamiltonian corresponding to $\tilde{S}$ = 1/2 (Kramers doublet in the case of Dy^{3+}, Ising doublet in the case of Tb^{3+}). Subsequently, diagonalizing the matrix representation of the Zeeman Hamiltonian gave us the magnetic anisotropy of the low-lying doublets on each Ln center.[62–64]

The final step is to take into account the exchange interaction *via* the superexchange model, which was implemented in the POLY_ANISO module.[65,66] Before applying the model, the molecules were rotated so that the exchange core obeyed D_{2h} symmetry as in Fig. 2(a) in ref. 31. Once the promotion energy U_0 was determined, the exchange parameters were fully derived. Accordingly, the exchange energy spectra and the magnetic properties of the polynuclear compounds were calculated. Based on the obtained data, the magnetization blocking diagrams were plotted for some low-lying exchange levels where the dominant relaxation paths occur.

4 Results and discussion

The local energy spectra and ground g-tensors are shown in Table 1. For the Dy complexes, without the THF, the local CF axiality is reduced considerably. In detail, the energy gap between the ground and first-excited Kramers doublets of **2-Dy** is 228 cm^{-1}, which is nearly a third smaller than that

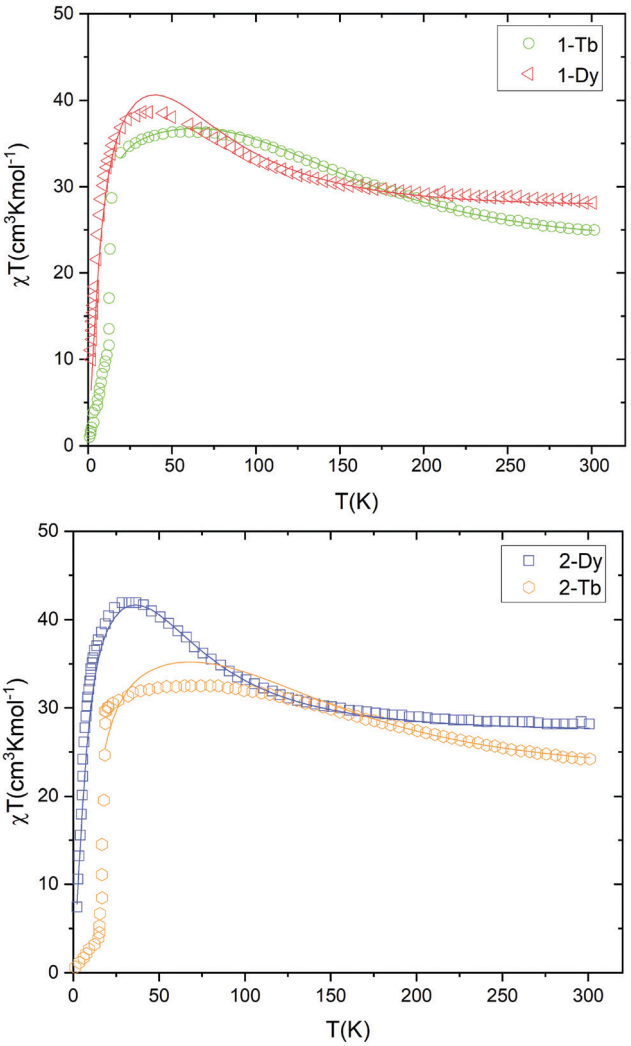

Fig. 2 Calculated (lines) and experimental (symbols) temperature-dependent magnetic susceptibility (χT) at H = 1 T.

of **1-Dy**. While their axial components (g_z) of the g-tensors are close to each other, the transverse components (g_x,g_y) of the former are an order of magnitude greater than the latter. Similarly, compared with **1-Tb**, the CF for **2-Tb** is also less axial due to the larger tunneling gap (Δ_{tun}) in the lowest Ising doublet. As a consequence, QTM is expected to be more pronounced when the THF is removed.[10,69] Therefore, for molecules possessing low symmetry, such as **1-Tb** and **1-Dy**, reducing the coordination number may not be a good strategy to promote the CF axiality.

The computed exchange parameters are shown in Table 3, once the promotion energy has been obtained by the fitting procedure (Table 2 and Fig. 2). We can see that the signs of the parameters are identical to those reported in ref. 31; and they are of the same order of magnitude. The reason is that due to the D_{2h} symmetry of the magnetic core, only the $4f_{xyz}$ orbitals are involved in the exchange process. As a result, the dominant first-rank terms $\mathcal{J}_{1q1q'}$ (q,q' = ±1) are isotropic instead of the usual non-Heisenberg type.[31] Therefore, the surrounding

Table 1 Energy structure of the ground J-multiplet and g-tensor of the ground doublet on each Ln center (cm^{-1})

State	1-Tb	1-Dy	2-Tb	2-Dy
1	0.000	0.000	0.000	0.000
2	0.033	0.000	0.049	0.000
3	131.475	298.283	207.267	228.062
4	131.551	298.283	207.784	228.062
5	290.473	427.562	441.542	288.807
6	292.557	427.562	445.238	288.807
7	428.059	510.644	641.997	342.790
8	448.955	510.644	684.420	342.790
9	519.793	593.428	817.791	418.417
10	583.151	593.428	844.855	418.417
11	599.365	683.648	902.363	485.687
12	822.600	683.648	1010.655	485.687
13	823.026	783.394	1015.901	579.703
14		783.394		579.703
15		893.778		813.933
16		893.778		813.933
g_x	0.0000	0.0048	0.0000	0.0202
g_y	0.0000	0.0076	0.0000	0.0385
g_z	17.8963	19.7382	17.8687	19.7973

Note that the transverse components of the g-tensor ($g_{x,y}$) of the Tb ion are zero because of Griffith's theorem.[67,68]

Table 2 Computational parameters and results obtained from the super-exchange model. Δ and t are the energy gap between the 4f–π* orbitals and the transfer parameter derived in the previous study, respectively.[31] U_0 is the minimal promotion energy. $g_{x,y,z}$ are the corresponding components of the g-tensor of the ground exchange doublet. θ is the angle between the magnetic anisotropy axes of the local and exchange ground doublets. U_{eff} is the blocking energy barrier obtained from the experiments[40] (exp.) and *ab initio* calculations (cal.). Unit of energy is cm^{-1}

	1-Tb	1-Dy	2-Tb	2-Dy
Δ	5.74×10^4	5.80×10^4	5.74×10^4	5.80×10^4
t	1333	1322	1333	1322
U_0	4100	6700	5000	5300
g_x	2.0×10^{-6}	1.9×10^{-5}	1.6×10^{-5}	6.5×10^{-4}
g_y	2.0×10^{-6}	3.3×10^{-5}	2.9×10^{-5}	1.2×10^{-3}
g_z	34	38	31	37
θ	8.3°	4.4°	0.4°	4.3°
(exp.) U_{eff1}	242	110	276	108
(cal.) U_{eff1}	240	104	222	113
(exp.) U_{eff2}	—	—	564	—
(cal.) U_{eff2}	—	208	440	210

ligands only influence slightly the nature of the exchange interaction provided by the radical, as expected. In addition, if the lanthanide ions are connected by other radical bridges in which the symmetry constraints are more permissive, other 4f orbitals might also participate in the magnetic coupling, enabling the anisotropy of the magnetic interaction.[31,70]

The diagram for magnetic relaxation is plotted in Fig. 3. As shown in the figure, the value of the matrix element of the transition magnetic moment within the ground exchange doublet in every complex is immensely small, indicating a significant suppression of QTM. For **1-Tb**, the number between −3 and +3 is equal to that between −4 and +4; and both of them are the largest. Hence, the most suitable path is *via* the latter since the transitions between −1 and −3 both directly and indirectly *via* the other states are relatively weak. On the other hand, for **1-Dy**, besides the relaxation path *via* the third level, there exists a possibility that the magnetization relaxes *via* the fourth one according to the toy model in Fig. 3b of ref. 31 as the admixture of the excited CF states to the four lowest exchange doublets is precluded (Fig. 3(b)). As a result, U_{eff} of **1-Tb** and **1-Dy** are 240 and 104 cm^{-1}, respectively, which are in a great agreement with the experimental data (Table 2).[40] On the other hand, for **2-Tb** and **2-Dy**, the value of the matrix element between −6 and +6 is similar to that between −2 and +2. Hence, in addition to the relaxation path *via* the second doublet, there may exist another path which involves the ±6 exchange levels, doubling the U_{eff} value of the former. In this scenario, the most relevant path is −1, −4, −6 then to the other side of the diagram which is highlighted by the orange arrows. Thus, the *ab initio* data confirm the experimental observation of two blocking energy barriers in **2-Tb**. It also suggests that not only **2-Tb** but also **1-Dy** and **2-Dy** possess the same property. The reason why the property is only observed in the former complex is perhaps that the measured temperature range in the Arrhenius plots for the latter two complexes is not sufficient: while for **1-Tb**, the temperature varies from 2 to 60 K, for **1-Dy** and **2-Dy**, they are 2–15 K and 2–18 K, respectively.[40]

Table 3 Computed exchange parameters $\mathcal{J}_{kq1q'}$

k	q	q'	1-Tb	2-Tb	Tb	1-Dy	2-Dy	Dy
1	0	0	104.7	89.8	95.8	68.9	85.3	70.8
1	±1	∓1	−104.7	−89.8	−95.8	−68.9	−85.3	−70.8
3	0	0	15.2	12.2	13.4	−10.3	−12.9	−10.6
3	±1	∓1	9.3	7.5	8.2	−6.3	−7.9	−6.5
3	±3	∓3	12.0	9.7	10.6	−8.1	−10.2	−8.4
5	0	0	19.3	15.5	17.0	−15.5	−19.7	−16
5	±1	∓1	−14.6	−11.7	−12.8	8.2	10.2	8.4
5	±3	∓3	−2.8	−2.3	−2.5	7.3	9.3	7.5
5	±4	∓4	6.5	5.2	5.7	−0.8	−0.8	−0.8
5	±5	∓5	−15.3	−12.3	−13.5	11.1	14.0	11.5
7	0	0	0.3	0.2	0.3	−3.2	−4.1	−3.3
7	±1	∓1	−0.2	−0.2	−0.2	2.4	3.1	2.5
7	±3	∓3	0.2	0.2	0.2	−2.1	−2.7	−2.2
7	±4	∓4	−0.5	−0.4	−0.4	4.9	6.3	5.1
7	±5	∓5	0.6	0.5	0.6	−6.9	−9.0	−7.2

Note that **Tb** and **Dy** are the complexes theoretically investigated in ref. 31.

Notably, the experimental data show that the barrier height of the Tb complexes is around twice as large as the Dy analogues, which is also confirmed by our calculations. Furthermore, this property also appeared in the previous series reported by Rinehart *et al.*[31–33] Since the surrounding ligands and the bridging radical are identical for the two lanthanide ions, it is predicted that the discrepancy may arise from the lanthanide sites themselves. To shed some light on this, the nature of the exchange levels are analyzed explicitly such that the contribution of the local state k on each magnetic center to the exchange level n is calculated as:

$$w(n,k) = \sum_{k',k''} |\langle k,k',k''|n\rangle|^2, \quad (6)$$

where $|k,k',k''\rangle$ are direct products of the local states of the three magnetic centers (Fig. 3 and Tables S1–S4, ESI†).

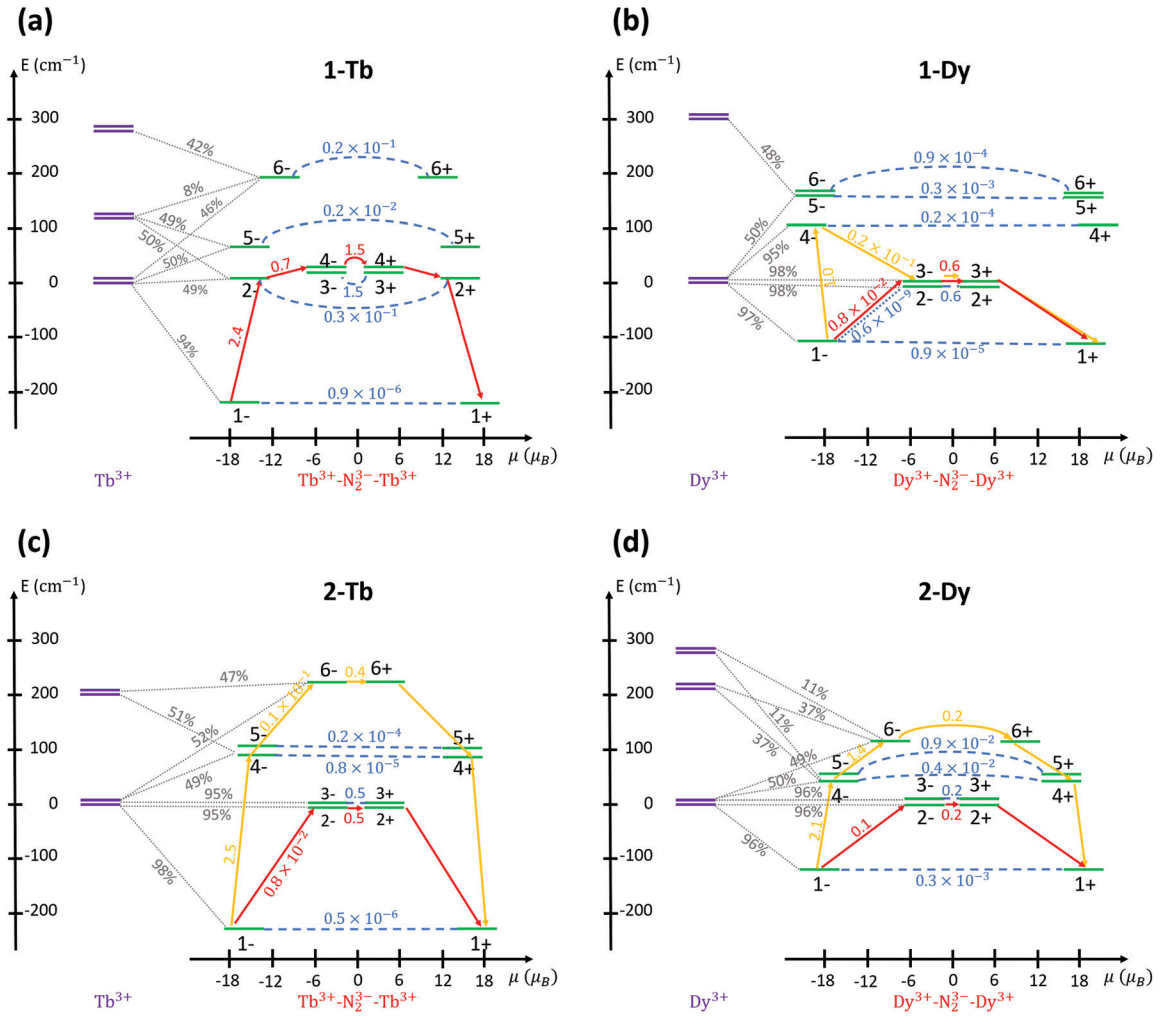

Fig. 3 Magnetization blocking barriers for (a) **1-Tb**, (b) **1-Dy**, (c) **2-Tb** and (d) **2-Dy**. Purple bands indicate the CF doublets on each Ln center. Green bands show the exchange levels which are arranged according to their magnetic moments. Grey dot lines with percentages highlight the admixture of the CF doublets to the exchange ones (details in Tables S1–S4, ESI†). The number at each blue, red and orange dashed line or arrow is the average of the absolute values of the matrix elements of transition magnetic moments between the two connected states. Blue dashed lines within the ground doublets display QTM while those within the excited doublets are temperature-assisted QTM. Red and orange arrows demonstrate the first and second possible relaxation paths, respectively.

Considering the cases where the THF group is removed, the two lowest exchange levels are mostly mixed by the ground CF doublet so that the energy gap between them is mainly from the exchange interaction (Fig. 3(c) and (d)). Since their parameters appearing in the microscopic model (t, Δ and U_0) are similar to each other, their exchange splitting is supposed to be also in equivalence.[31,53,71] However, as shown in Table 4, the energy gap between the two lowest exchange doublets in **2-Tb** is around twice as large as that in **2-Dy**. This discrepancy, in fact, results from (i) the D_{2h} symmetry of the exchange core Ln^{3+}–N_2^{3-}–Ln^{3+} where the anti-bonding π* orbital of the radical overlaps with the $4f_{xyz}$ molecular orbital(s) corresponding to L, $M_L = 3, \pm 2$; and (ii) the superexchange originates from the transition of the unpaired electron *i.e.* $(4f)^n(\pi^*)^1 \Leftrightarrow (4f)^{n+1}(\pi^*)^0$. As a consequence, whereas in the Tb^{3+} ion there are two possible paths for the electron transition, in Dy^{3+}, the molecular orbital 3, 2 is already filled, leading to only one electron transfer path (Fig. 4). As a result, the exchange splitting in **2-Tb** is roughly twice as large as the corresponding value in **2-Dy**, which also offers a twofold energy gap between the ground and first excited doublets in **2-Tb** compared with **2-Dy**. Therefore, the blocking barrier in the Tb complex

Table 4 Energies of low-lying exchange doublets (cm^{-1})

Doublet	1-Tb	1-Dy	2-Tb	2-Dy
1	0.000	0.000	0.000	0.000
2	235.341	103.948	221.725	112.641
3	240.132	103.948	221.725	112.658
4	240.249	207.842	305.016	138.858
5	256.089	246.928	321.093	141.852
6	402.350	248.673	439.820	209.529
7	405.877	337.700	439.820	210.541
8	408.897	337.701	474.591	219.465
9	409.435	376.237	533.112	223.273

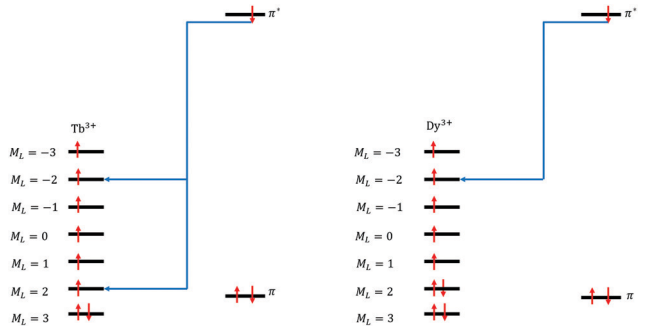

Fig. 4 The transition path(s) of the unpaired electron from the π^* orbital to the $4f_{xyz}$ orbital(s) in Tb^{3+} and Dy^{3+}. The splitting between orbitals is not drawn at its true scale, for clarity. The splitting between 4f orbitals is proportional to the CF splitting (10^2–10^3 cm^{-1}) while that between the π and π^* orbitals is estimated at about 10^4–10^5 cm^{-1}.

is approximately twice as large as in the Dy analogue, given that the most common relaxation path for the N_2^{3-}-containing dilanthanide series is *via* the first-excited exchange level.[31–33,40]

5 Conclusion

In this work, the top-performing N_2^{3-}-bridged dilanthanide compounds reported in ref. 40 were investigated by using a combination of an *ab initio* approach and an adequate theoretical model of magnetic exchange interaction. On the basis of the obtained results, the magnetic blocking behavior and the origin of the two blocking barriers in the series were elucidated. For performant SIMs, the Dy^{3+} ion is undoubtedly more favorable than the Tb^{3+} ion given that the former possesses a larger magnetic moment. However, the situation becomes more complex when the exchange interaction enters into the equation. In the case of Ln^{3+}–N_2^{3-}–Ln^{3+}, the effective blocking barrier U_{eff} of Tb compounds is around twice as large as the U_{eff} of the Dy analogues due to the fact that the exchange splitting in the former is approximately double that of the latter. Therefore, if the exchange interaction is promoted by the N_2^{3-} radical, Tb ions have a better potential to improve the SMM performance compared with other Ln ions. This rule is not only applicable for this family but also possibly to any complexes whose exchange core possesses D_{2h} symmetry. Besides the magnetic core, the design of the surrounding ligands also represents an important step towards the enhancement of exchange magnetization blockage. Future work will certainly concentrate on this aspect to further elucidate the microscopic picture of exchange-coupled lanthanide complexes.

Conflicts of interest

There are no conflicts to declare.

Acknowledgements

G. T. N. was supported by the NUS Research Scholarship program. We acknowledge the financial support of the research projects R-143-000-A65-133 and R-143-000-A80-114 of the National University of Singapore. *Ab initio* calculations were done on the ASPIRE-1 cluster (www.nscc.sg) under the project 11001278. We would like to thank Dr. Naoya Iwahara for useful discussions.

References

1 A. Caneschi, D. Gatteschi, R. Sessoli, A. L. Barra, L. C. Brunel and M. Guillot, *J. Am. Chem. Soc.*, 1991, **113**, 5873–5874.
2 R. Sessoli, D. Gatteschi, A. Caneschi and M. Novak, *Nature*, 1993, **365**, 141–143.
3 P. Gambardella, S. Stepanow, A. Dmitriev, J. Honolka, F. M. De Groot, M. Lingenfelder, S. S. Gupta, D. Sarma, P. Bencok and S. Stanescu, *et al.*, *Nat. Mater.*, 2009, **8**, 189–193.
4 L. Ungur, S.-Y. Lin, J. Tang and L. F. Chibotaru, *Chem. Soc. Rev.*, 2014, **43**, 6894–6905.
5 H. B. Heersche, Z. de Groot, J. A. Folk, H. S. J. van der Zant, C. Romeike, M. R. Wegewijs, L. Zobbi, D. Barreca, E. Tondello and A. Cornia, *Phys. Rev. Lett.*, 2006, **96**, 206801.
6 L. Bogani and W. Wernsdorfer, *Nat. Mater.*, 2008, **7**, 179–186.
7 M. N. Leuenberger and D. Loss, *Nature*, 2001, **410**, 789–793.
8 G. A. Timco, S. Carretta, F. Troiani, F. Tuna, R. J. Pritchard, C. A. Muryn, E. J. McInnes, A. Ghirri, A. Candini and P. Santini, *et al.*, *Nat. Nanotechnol.*, 2009, **4**, 173.
9 G. Arom, D. Aguila, P. Gamez, F. Luis and O. Roubeau, *Chem. Soc. Rev.*, 2012, **41**, 537–546.
10 D. Gatteschi, R. Sessoli and J. Villain, *Molecular Nanomagnets*, Oxford University Press, Oxford, 2006.
11 N. Ishikawa, M. Sugita, T. Ishikawa, S.-Y. Koshihara and Y. Kaizu, *J. Am. Chem. Soc.*, 2003, **125**, 8694–8695.
12 S. Takamatsu, T. Ishikawa, S.-Y. Koshihara and N. Ishikawa, *Inorg. Chem.*, 2007, **46**, 7250–7252.
13 M. Gonidec, F. Luis, A. Vilchez, J. Esquena, D. Amabilino and J. Veciana, *Angew. Chem., Int. Ed.*, 2010, **49**, 1623–1626.
14 R. Westerström, J. Dreiser, C. Piamonteze, M. Muntwiler, S. Weyeneth, H. Brune, S. Rusponi, F. Nolting, A. Popov, S. Yang, L. Dunsch and T. Greber, *J. Am. Chem. Soc.*, 2012, **134**, 9840–9843.
15 R. J. Blagg, L. Ungur, F. Tuna, J. Speak, P. Comar, D. Collison, W. Wernsdorfer, E. J. McInnes, L. F. Chibotaru and R. E. Winpenny, *Nat. Chem.*, 2013, **5**, 673–678.
16 S. K. Langley, D. P. Wielechowski, V. Vieru, N. F. Chilton, B. Moubaraki, B. F. Abrahams, L. F. Chibotaru and K. S. Murray, *Angew. Chem., Int. Ed.*, 2013, **52**, 12014–12019.
17 S. K. Langley, D. P. Wielechowski, V. Vieru, N. F. Chilton, B. Moubaraki, L. F. Chibotaru and K. S. Murray, *Chem. Sci.*, 2014, **5**, 3246–3256.
18 L. Ungur, J. J. LeRoy, I. Korobkov, M. Murugesu and L. F. Chibotaru, *Angew. Chem., Int. Ed.*, 2014, **53**, 4413–4417.

19 Y.-C. Chen, J.-L. Liu, L. Ungur, J. Liu, Q.-W. Li, L.-F. Wang, Z.-P. Ni, L. F. Chibotaru, X.-M. Chen and M.-L. Tong, *J. Am. Chem. Soc.*, 2016, **138**, 2829–2837.
20 J. Liu, Y.-C. Chen, J.-L. Liu, V. Vieru, L. Ungur, J.-H. Jia, L. F. Chibotaru, Y. Lan, W. Wernsdorfer, S. Gao, X.-M. Chen and M.-L. Tong, *J. Am. Chem. Soc.*, 2016, **138**, 5441–5450.
21 C. A. Goodwin, F. Ortu, D. Reta, N. F. Chilton and D. P. Mills, *Nature*, 2017, **548**, 439–442.
22 F.-S. Guo, B. M. Day, Y.-C. Chen, M.-L. Tong, A. Mansikkamäki and R. A. Layfield, *Angew. Chem., Int. Ed.*, 2017, **56**, 11445–11449.
23 K. Randall McClain, C. A. Gould, K. Chakarawet, S. J. Teat, T. J. Groshens, J. R. Long and B. G. Harvey, *Chem. Sci.*, 2018, **9**, 8492–8503.
24 F.-S. Guo, B. M. Day, Y.-C. Chen, M.-L. Tong, A. Mansikkamäki and R. A. Layfield, *Science*, 2018, **362**, 1400–1403.
25 L. Ungur and L. F. Chibotaru, *Phys. Chem. Chem. Phys.*, 2011, **13**, 20086–20090.
26 N. F. Chilton, *Inorg. Chem.*, 2015, **54**, 2097–2099.
27 L. Ungur and L. F. Chibotaru, *Inorg. Chem.*, 2016, **55**, 10043–10056.
28 Y.-N. Guo, G.-F. Xu, W. Wernsdorfer, L. Ungur, Y. Guo, J. Tang, H.-J. Zhang, L. F. Chibotaru and A. K. Powell, *J. Am. Chem. Soc.*, 2011, **133**, 11948–11951.
29 W. Wernsdorfer, N. Aliaga-Alcalde, D. N. Hendrickson and G. Christou, *Nature*, 2002, **416**, 406–409.
30 S. Demir, I.-R. Jeon, J. R. Long and T. D. Harris, *Coord. Chem. Rev.*, 2015, **289–290**, 149–176.
31 V. Vieru, N. Iwahara, L. Ungur and L. F. Chibotaru, *Sci. Rep.*, 2016, **6**, 24046.
32 J. D. Rinehart, M. Fang, W. J. Evans and J. R. Long, *Nat. Chem.*, 2011, **3**, 538–542.
33 J. D. Rinehart, M. Fang, W. J. Evans and J. R. Long, *J. Am. Chem. Soc.*, 2011, **133**, 14236–14239.
34 K. Prša, J. Nehrkorn, J. F. Corbey, W. J. Evans, S. Demir, J. R. Long, T. Guidi and O. Waldmann, *Magnetochemistry*, 2016, **2**, 45.
35 F.-S. Guo and R. A. Layfield, *Chem. Commun.*, 2017, **53**, 3130–3133.
36 S. Demir, J. M. Zadrozny, M. Nippe and J. R. Long, *J. Am. Chem. Soc.*, 2012, **134**, 18546–18549.
37 S. Demir, M. Nippe, M. I. Gonzalez and J. R. Long, *Chem. Sci.*, 2014, **5**, 4701–4711.
38 B. S. Dolinar, S. Gómez-Coca, D. I. Alexandropoulos and K. R. Dunbar, *Chem. Commun.*, 2017, **53**, 2283–2286.
39 C. A. Gould, L. E. Darago, M. I. Gonzalez, S. Demir and J. R. Long, *Angew. Chem., Int. Ed.*, 2017, **56**, 10103–10107.
40 S. Demir, M. I. Gonzalez, L. E. Darago, W. J. Evans and J. R. Long, *Nat. Commun.*, 2017, **8**, 1–9.
41 M. A. Dunstan, E. Rousset, M.-E. Boulon, R. W. Gable, L. Sorace and C. Boskovic, *Dalton Trans.*, 2017, **46**, 13756–13767.
42 P. Zhang, M. Perfetti, M. Kern, P. P. Hallmen, L. Ungur, S. Lenz, M. R. Ringenberg, W. Frey, H. Stoll, G. Rauhut and J. van Slageren, *Chem. Sci.*, 2018, **9**, 1221–1230.
43 W. R. Reed, M. A. Dunstan, R. W. Gable, W. Phonsri, K. S. Murray, R. A. Mole and C. Boskovic, *Dalton Trans.*, 2019, **48**, 15635–15645.
44 M. A. Hay and C. Boskovic, *Chem. – Eur. J.*, 2021, **27**, 1–31.
45 M. Murugesu, N. Mavragani, A. A. Kitos and J. L. Brusso, *Chem. – Eur. J.*, 2021, **27**, 1–17.
46 L. Ungur and L. F. Chibotaru, *Chem. – Eur. J.*, 2017, **23**, 3708–3718.
47 N. Iwahara, L. Ungur and L. F. Chibotaru, *Phys. Rev. B*, 2018, **98**, 054436.
48 D. A. Varshalovich, A. N. Moskalev and V. K. Khersonskii, *Quantum Theory of Angular Momentum*, World Scientific, Singapore, 1988.
49 R. J. Elliott and M. F. Thorpe, *J. Appl. Phys.*, 1968, **39**, 802.
50 F. Hartmann-Boutron, *J. Phys.*, 1968, **29**, 212.
51 P. Santini, S. Carretta, G. Amoretti, R. Caciuffo, N. Magnani and G. H. Lander, *Rev. Mod. Phys.*, 2009, **81**, 807.
52 N. Iwahara and L. F. Chibotaru, *Phys. Rev. B: Condens. Matter Mater. Phys.*, 2015, **91**, 174438.
53 P. W. Anderson, *Phys. Rev.*, 1959, **115**, 2–13.
54 D. Khomskii, *Transition metal compounds*, Cambridge University Press, 2014.
55 J. B. Goodenough, *Magnetism and the chemical bond*, Interscience publishers, 1963, vol. 1.
56 I. F. Galvan, M. Vacher, A. Alavi, C. Angeli, F. Aquilante, J. Autschbach, J. J. Bao, S. I. Bokarev, N. A. Bogdanov, R. K. Carlson, L. F. Chibotaru, J. Creutzberg, N. Dattani, M. G. Delcey, S. S. Dong, A. Dreuw, L. Freitag, L. M. Frutos, L. Gagliardi, F. Gendron, A. Giussani, L. Gonzalez, G. Grell, M. Guo, C. E. Hoyer, M. Johansson, S. Keller, S. Knecht, G. Kovacevic, E. Kallman, G. Li Manni, M. Lundberg, Y. Ma, S. Mai, J. P. Malhado, P. A. Malmqvist, P. Marquetand, S. A. Mewes, J. Norell, M. Olivucci, M. Oppel, Q. M. Phung, K. Pierloot, F. Plasser, M. Reiher, A. M. Sand, I. Schapiro, P. Sharma, C. J. Stein, L. K. Sorensen, D. G. Truhlar, M. Ugandi, L. Ungur, A. Valentini, S. Vancoillie, V. Veryazov, O. Weser, T. A. Wesolowski, P.-O. Widmark, S. Wouters, A. Zech, J. P. Zobel and R. Lindh, *J. Chem. Theory Comput.*, 2019, **15**, 5925–5964.
57 F. Aquilante, J. Autschbach, R. K. Carlson, L. F. Chibotaru, M. G. Delcey, L. De Vico, I. F. Galvan, N. Ferre, L. M. Frutos, L. Gagliardi, M. Garavelli, A. Giussani, C. E. Hoyer, G. Li Manni, H. Lischka, D. Ma, P. A. Malmqvist, T. Muller, A. Nenov, M. Olivucci, T. B. Pedersen, D. Peng, F. Plasser, B. Pritchard, M. Reiher, I. Rivalta, I. Schapiro, J. Segarra-Marti, M. Stenrup, D. G. Truhlar, L. Ungur, A. Valentini, S. Vancoillie, V. Veryazov, V. P. Vysotskiy, O. Weingart, F. Zapata and R. Lindh, *J. Comput. Chem.*, 2016, **37**, 506–541.
58 A. L. Spek, *Acta Crystallogr., Sect. C: Struct. Chem.*, 2015, **71**, 9–18.
59 B. O. Roos, R. Lindh, P.-A. Malmqvist, V. Veryazov, P.-O. Widmark and A. C. Borin, *J. Phys. Chem. A*, 2008, **112**, 11431–11435.
60 P. A. Malmqvist, B. O. Roos and B. Schimmelpfennig, *Chem. Phys. Lett.*, 2002, **357**, 230–240.

61 L. F. Chibotaru and L. Ungur, *J. Chem. Phys.*, 2012, **137**, 064112.
62 L. F. Chibotaru, *Ab Initio Methodology for Pseudospin Hamiltonians of Anisotropic Magnetic Complexes*, John Wiley & Sons, Ltd, 2013, pp. 397–519.
63 L. Ungur and L. F. Chibotaru, *Computational Modelling of the Magnetic Properties of Lanthanide Compounds*, John Wiley & Sons, Ltd, 2015, ch. 6, pp. 153–184.
64 L. Chibotaru, *Struct. Bonding*, 2014, **164**, 185–230.
65 L. F. Chibotaru and L. Ungur, *The computer programs SINGLE_ANISO and POLY_ANISO*, University of Leuven, 2006.
66 L. Ungur and L. F. Chibotaru, *Computational Modelling of the Magnetic Properties of Lanthanide Compounds*, John Wiley & Sons, Ltd, 2015, ch. 6, pp. 153–184.
67 J. S. Griffith, *Phys. Rev.*, 1963, **132**, 316–319.
68 J. S. Griffith, *The Theory of Transition-Metal Ions*, Cambridge University Press, 1964.
69 C. Sangregorio, T. Ohm, C. Paulsen, R. Sessoli and D. Gatteschi, *Phys. Rev. Lett.*, 1997, **78**, 4645–4648.
70 T. Moriya, *Phys. Rev.*, 1960, **120**, 91.
71 P. W. Anderson, *Solid state physics*, Elsevier, 1963, vol. 14, pp. 99–214.

